Atmos. Chem. Phys. Discuss., 11, 28851–28894, 2011
www.atmos-chem-phys-discuss.net/11/28851/2011/
doi:10.5194/acpd-11-28851-2011

Atmospheric Chemistry and Physics Discussions

Comparisons of observed and modeled OH and HO_2 concentrations during the ambient measurement period of the HO_xComp field campaign

Y. Kanaya[1], A. Hofzumahaus[2], H.-P. Dorn[2], T. Brauers[2], H. Fuchs[2], F. Holland[2], F. Rohrer[2], B. Bohn[2], R. Tillmann[2], R. Wegener[2], A. Wahner[2], Y. Kajii[3], K. Miyamoto[3], S. Nishida[3,*], K. Watanabe[3], A. Yoshino[3,], D. Kubistin[4], M. Martinez[4], M. Rudolf[4], H. Harder[4], H. Berresheim[5,***], T. Elste[5], C. Plass-Dülmer[5], G. Stange[5], J. Kleffmann[6], Y. Elshorbany[6,****], and U. Schurath[7]**

[1]Research Institute for Global Change (formerly FRCGC), Japan Agency for Marine–Earth Science and Technology, Yokohama 236-0001, Japan
[2]Forschungszentrum Jülich, IEK-8: Troposphäre, 52425 Jülich, Germany
[3]Tokyo Metropolitan University, Department of Applied Chemistry, Tokyo 192-0397, Japan

[4] Max Planck Institute for Chemistry, Atmospheric Chemistry Department, 55020 Mainz, Germany
[5] Deutscher Wetterdienst, Meteorologisches Observatorium, 82383 Hohenpeissenberg, Germany
[6] Bergische Universität Wuppertal, 42097 Wuppertal, Germany
[7] Karlsruhe Institute of Technology (KIT), IMK-AAF, 76021 Karlsruhe, Germany
[*] now at: Gifu University, Gifu 501-1193, Japan
[**] now at: Tokyo University of Agriculture and Technology, Tokyo 183-8538, Japan
[***] now at: National University of Ireland Galway, Department of Physics, Galway, Ireland
[****] now at: Max Planck Institute for Chemistry, Atmospheric Chemistry Department, 55020 Mainz, Germany

Received: 21 September 2011 – Accepted: 15 October 2011 – Published: 26 October 2011

Correspondence to: Y. Kanaya (yugo@jamstec.go.jp)

ACPD
11, 28851–28894, 2011

Abstract

A photochemical box model constrained by ancillary observations was used to simulate OH and HO_2 concentrations for three days of ambient observations during the HO_xComp field campaign held in Jülich, Germany in July 2005. OH and HO_2 levels, observed by four and three instruments, respectively, were fairly well reproduced to within 33 % by a base model run (Regional Atmospheric Chemistry Mechanism with updated isoprene chemistry adapted from Master Chemical Mechanism ver. 3.1) with high R^2 values (0.72–0.97) over a range of isoprene (0.3–2 ppb) and NO (0.1–10 ppb) mixing ratios. Adding isomerization of isoprene peroxy radicals to the model increased OH and HO_2 by 43 % and 48 % on average. Although these are still only 15 % and 21 % higher than the observations made by one of the instruments, larger overestimations (> 60 %) occurred with respect to the observations made by the other three instruments, suggesting that the rates of the isomerization were not readily supported by the ensemble of radical observations. These model runs tend to underestimate observed OH reactivity which may be explained by unmeasured hydrocarbon species. By selecting hydrocarbon types to be added to the model in amounts that accounted for the missing fractions of observed OH reactivity, the gaps between HO_x observations and model results with and without isomerization could be individually diminished to within uncertainty levels. In this case, however, the HO_2/OH ratio rose on addition of hydrocarbons and diverged from observations. In the case where we used modeled HO_2(*), taking into account the sensitivity toward speciated RO_2 (organic peroxy) radicals, as recently reported from one of the participating instruments in the HO_2 measurement mode, the model's overestimation for HO_2 became evident (by factors of more than 1.8). These results strongly indicated that more loss processes for peroxy radicals were necessary to explain the observations. One of the measurement days was characterized by low isoprene concentrations (~ 0.5 ppb) and OH reactivity that was well explained by the observed species, especially before noon. For this selected period, as opposed to the general behavior, the model tended to underestimate HO_2

ACPD
11, 28851–28894, 2011

(and HO_2(*)) with respect to observations made by the three instruments. We found that this tendency is associated with high NO_x concentrations, suggesting that some HO_2 production or HO_2 regeneration processes under high NO_x conditions were being overlooked; this might require revision of ozone production regimes.

1 Introduction

Reactions of OH and HO_2 radicals in the troposphere constitute the basis of the chemical mechanisms explaining photochemical ozone production and formation of acidic species. Fundamental radical reactions also control the behaviors of important chemical species related to global climate change (e.g., methane). Comparisons of modeled and observed tropospheric OH and HO_2 radical concentrations have served as effective tests of our current understanding of tropospheric chemistry mechanisms. Past comparisons near the Earth's surface and in the air above led to the identification of new processes essential to the budget of HO_x ($OH + HO_2$) radicals; these processes had previously been missing from our knowledge (e.g., acetone photolysis, Wennberg et al., 1998). Although they may not lead to an immediate clarification of processes, the accumulation of these comparisons at multiple sites is important for the identification of common tendencies. For example, HO_2 concentrations are overestimated in clean coastal regions (Sommariva et al., 2004; Kanaya et al., 2007a), and this assists systematic surveying of the processes responsible for the discrepancies. Recent observations revealed that OH concentrations under high volatile organic compound (VOC) and low NO_x conditions were systematically larger than the modeled concentrations. Hofzumahaus et al. (2009) and Lu et al. (2011) suggested that unidentified processes converting RO_2 to HO_2 and HO_2 to OH have an effect in a rural area in the Pearl River Delta (PRD), China. Martinez et al. (2010), Kubistin et al. (2010), and Ren et al. (2008) found that OH and HO_2 radical concentrations measured by aircraft over Suriname and the Eastern United States were higher than those modeled in the planetary boundary layer when accompanied by high isoprene concentrations

ACPD
11, 28851–28894, 2011

emitted from the terrestrial biosphere. Recently, three-dimensional chemical transport models (Peeters and Müller, 2010; Stavrakou et al., 2010; Archibald et al., 2010) explained the high radical concentration levels observed in regions of biosphere influence at least qualitatively using isomerization of isoprene peroxy radicals, basically as proposed by theoretical studies (Peeters et al., 2009; Peeters and Müller, 2010). Whalley et al. (2011) and Pugh et al. (2010) reported similar underestimation for OH by a model in tropical forests.

Recent measurements of OH reactivity have added a new dimension to the diagnosis of the HO_x chemistry. A fraction of the observed reactivity is sometimes left unexplained by the sum of reactivities contributed from known gas species present in the atmosphere, suggesting the existence of unmeasured species that contribute to OH loss (Di Carlo et al., 2004; Sadanaga et al., 2005; Yoshino et al., 2006). Thus, the knowledge of a robust set of reactions that reasonably explain both OH reactivity and radical concentrations is still an open issue. The studies focusing on this issue contribute to a better understanding, and improvements in the predictive capabilities of various atmospheric phenomena that are based on fundamental radical chemistry.

Because only a few research groups have performed tropospheric OH and HO_2 observations, in the past, HO_x measurements were normally made by a single instrument during individual campaigns, and such observations were compared with theoretical values. The HO_xComp field campaign (Schlosser et al., 2009; Fuchs et al., 2010) was an exceptional and unique opportunity: OH and HO_2 concentrations were measured with multiple instruments, and thus more reliable comparisons with model results could be made. Schlosser et al. (2009) reported that ambient OH levels measured by four instruments correlated strongly (R^2 ranged from 0.75 to 0.96), and that the slopes of pairwise linear regressions were between 1.06 and 1.69 (with negligible intercepts); this can be partly explained by the stated instrumental accuracies. They argue that sampling inhomogeneities and calibration problems have contributed to the discrepancies. Fuchs et al. (2010) stated that ambient daytime HO_2 levels, measured by three instruments, correlated with each other even more strongly (R^2 ranged from 0.92 to

ACPD
11, 28851–28894, 2011

0.98), with a similar range of linear-regression slopes (1.19–1.69) and with small intercepts. However, a systematic sensitivity difference, which was dependent on the amount of water vapor and was noticed in comparisons with chamber air, would also affect ambient measurements. Again, the slope values can only be partly explained by the combined 1σ accuracies of the calibrations. Here, we evaluate the degrees of agreement between the observed OH and HO_2 concentrations and theoretical values predicted using a photochemical box model. By changing the set of reactions used in the model, we examine the impact of the isomerization of isoprene peroxy radicals. We also study the tendency, found in measurements of HO_2 levels with three instruments, for models to underestimate HO_2 levels at high NO levels. Outlines of the experiments are described briefly in Sect. 2, followed by a detailed explanation of the model simulations in Sect. 3. Results and discussion are given in Sect. 4. In another forthcoming paper (Elshorbany et al., 2011), a detailed analysis of the HO_x radical budgets, secondary radical balance and turnover rates as well as the impact of HONO on the radical chemistry on 10 July 2005, using the master chemical mechanism (MCM), is presented.

2 Experimental and ambient air conditions

HO_xComp was designed to compare HO_x measurements performed by different instruments in a blind intercomparison under well characterized atmospheric chemical conditions. Details of the HO_xComp have been described by Schlosser et al. (2009) and Fuchs et al. (2010). In this paper, daytime data during the ambient observation period (9–11 July 2005) are analyzed in detail. The measurement site on the campus of Forschungszentrum Jülich (50°54′33″ N, 06° 24′44″ E) is located in a mixed deciduous forest (Stetternicher Forst) in a rural area close to Jülich, Germany. The forest area around the campus has an extension of about 1 km in the wind direction encountered during the three days, and consists mainly of oak, birch, and beech. A chemical ionization mass spectrometry (CIMS) instrument from Deutscher Wetterdienst

ACPD
11, 28851–28894, 2011

(DWD) measured OH levels (Berresheim et al., 2000; Rohrer and Berresheim, 2006). Three laser-induced fluorescence (LIF) instruments, from the Frontier Research Center for Global Change (FRCGC) (Kanaya et al., 2001; Kanaya and Akimoto, 2006), Forschungszentrum Jülich (FZJ) (Lu et al., 2011; Fuchs et al., 2011), and the Max Planck Institute (MPI) (Martinez et al., 2010), measured OH and HO_2 concentrations. Each instrument was calibrated by its own system. The instruments were housed in containers and set up on the paved area between the institute building and the SAPHIR chamber. The instruments were separated by 2.7–4.5 m (see Fig. 1 of Schlosser et al., 2009). All the OH and HO_2 measurements were made by sampling ambient air at approximately equal heights (3.5 m) above the ground. The detection limits and uncertainties for the OH and HO_2 observations are summarized in Table 1. The HO_2/OH ratio for the FRCGC instrument, where OH and HO_2 were detected in the same single cell alternately and thus systematic uncertainties in OH and HO_2 measurements arising from calibration are common and cancel out, had a smaller uncertainty, ±6 % (1σ), estimated from the temporal variations in the HO_2-to-OH conversion efficiency determined during the calibrations for the whole campaign period. The OH and HO_2 data without quality flags (used as markers to indicate "not valid" by each group) were averaged for 10-min intervals and used for the analysis. The observed HO_2/OH ratios were used for analysis only when HO_2 and OH measurements were made at least once and twice, respectively, in the pertinent 10-min period, and the averaged OH concentrations exceeded 1×10^6 and 5×10^5 radicals cm^{-3} in the daylight period (04:00–19:00 UTC) and nighttime (other period), respectively.

Recently, Fuchs et al. (2011) showed that HO_2 measurements with the FZJ instrument suffered from a large interference by specific RO_2 radicals. They pointed out that this is a potential problem in all instruments which detect HO_2 by chemical conversion to OH. In fact, a similar large interference was confirmed experimentally for the MPI instrument (Dillon, 2011). In Table 1, such uncertainty is not taken into account. In this paper, this influence on the analysis of HO_2 and HO_2/OH will be discussed in detail in Sect. 4.5.

ACPD
11, 28851–28894, 2011

The OH reactivity was measured with an instrument using a pump-and-probe method developed by Tokyo Metropolitan University (Sadanaga et al., 2005; Yoshino et al., 2006) by sampling ambient air at similar heights. The uncertainty in the reactivity data during this field campaign was estimated to be 15 %.

Standard instruments recorded humidity, ozone, and meteorological data. The ambient temperature was moderate, peaking at 28 °C on 10 July. On 9 July, ground fog was present until 08:10 UTC and later it was sunny with scattered clouds. It was almost cloud-free on 10 July. Although it was sunny until 14:00 on 11 July, a rainstorm occurred after that. NO and NO_2 were measured using an instrument from Eco Physics (Duernten, Switzerland). CO was measured by a GC-RGD (gas chromatography/reduction gas detector). $J(O^1D)$, $J(NO_2)$, $J(HONO)$, $J(HCHO)_{radical}$, $J(HCHO)_{molecule}$, and $J(H_2O_2)$ were determined with a spectral actinic flux radiometer. See Fig. 3 of Schlosser et al. (2009) and Fig. 2 of Fuchs et al. (2010) for NO_x, O_3, and $J(O^1D)$ values. Briefly, ozone concentrations showed similar daytime peaks (62–65 ppb) for all three days. NO showed morning peaks of about 12, 2, and 5 ppb on the three days (see also Fig. S1). It should be noted that NO reached a level as low as 0.17 ppb during 12:00–16:00 UTC on 10 July (Sunday). HONO was measured by a long path absorption photometer (Heland et al., 2001; Kleffmann et al., 2005). HONO showed a typical diurnal variation with highest concentrations around sunrise (300–600 ppt) and lower concentrations (80–160 ppt) in the early afternoon (12:00–15:00 UTC). Multiple GC systems measured non-methane hydrocarbons and other VOCs at a frequency of 50 min. These included ethane, ethene, acetylene, propane, propene, isobutane, isobutene, but-1-ene, *trans*-butene, isopentane, *n*-pentane, *cis*-2-pentene, *n*-hexane, *n*-heptane, *n*-octane, *n*-decane, benzene, toluene, ethylbenzene, *o*-xylene, *m*-xylene, *p*-xylene, butanal, butanone, isoprene, methacrolein (MACR), methyl vinyl ketone (MVK), propanal, acetone, and acetaldehyde. Isoprene concentrations showed diurnal variations, with daytime maxima. The average midday (09:00–15:00 UTC) isoprene concentrations were 0.45, 0.71, and 1.16 ppb for the three days (see Fig. S1). A maximum isoprene concentration (2.4 ppb) was recorded at 15:21 UTC

ACPD
11, 28851–28894, 2011

on 11 July. HCHO was measured using a Hantzsch AL-4001 monitor (Aero-Laser, Garmisch-Partenkirchen, Germany). Typical midday concentrations were 2–3 ppb. Measurement uncertainties of the trace gases are listed in Table S2. The sunrise, local noon, and sunset occurred at 3:34–3:36, 11:39, and 19:43–19:45 UTC, respectively.

3 Model simulations

The photochemical box model we used is based on the regional atmospheric chemistry mechanism (RACM) designed by Stockwell et al. (1997), but the isoprene chemistry is revised for the base run, as shown in Table S1 (except A7–10 reactions). The revision is in line with MCM ver. 3.1 (http://mcm.leeds.ac.uk/MCM/). The reaction pathways are shown in Fig. 1. In the base run, isomerization of isoprene peroxy radicals is not taken into account, but formation of epoxides (Paulot et al., 2008) is incorporated. Kinetic parameters and product yields of the mechanism were mainly taken from Pöschl et al. (2000), Peeters and Müller (2010), Stavrakou et al. (2010), Taraborrelli et al. (2009), and Paulot et al. (2008). The advantages over the original RACM are that MVK is taken into account separately and that a third product (HALD5152) represents unmeasured secondary species, even if MACR and MVK are both constrained to observations. Several kinetic parameters and yields in the original RACM were also revised: the rate coefficients of the $O(^1D) + N_2$ and $OH + NO_2 + M$ reactions were taken from Ravishankara et al. (2002) and MCM ver. 3.1, respectively. OH production from acylperoxy + HO_2 radical reactions, recently proved by Dillon and Crowley (2008), was taken into account. The rate coefficients of the $RO_2 + NO$ and $RO_2 + HO_2$ reactions (except peroxy radicals from methane, ethane and ethene and acylperoxy radicals) were taken from MCM ver. 3.1. The dry deposition velocities of H_2O_2, HNO_3, carbonyl species, peroxyacyl nitrates, nitrates, and organic peroxides were assumed to be 1.1, 2.0, 0.5, 0.2, 1.1, and 0.55 cm s^{-1}, respectively (Brasseur et al., 1998; Zhang et al., 2003). The change in the boundary layer height (300 m during nighttime, linear increase to 1300 m from 06:00 to 14:00 UTC, constant at 1300 m until 19:50 UTC, and

ACPD
11, 28851–28894, 2011

an immediate drop to 300 m at 19:50 UTC) was taken into account in representing the deposition loss flux.

All of the ancillary observations were averaged or interpolated with a time resolution of 10 min and used as model constraints. Data gaps were basically filled by linear interpolation. Photolysis frequencies other than those directly measured were estimated. In detail, clear-sky values were first calculated by using parameterized equations as functions of the solar zenith angle and then they were multiplied by a "cloudiness factor", defined as the ratio of measured $J(NO_2)$ to calculated clear-sky $J(NO_2)$. A multiplication factor of 1.05 was used to account for upwelling fractions of J values.

The model framework has been outlined elsewhere (Kanaya et al., 2007a). A model calculation was made for each day. The time 00:00 UTC was regarded as the initial time on each day, and integration over 24 h was conducted by 10-min binning of the data. This integration was conducted five times in series to stabilize the concentrations of unconstrained species (e.g., unmeasured carbonyl and peroxide species). The results for the last 24 h were used as the output for each day. However, this general time-dependent approach resulted in MACR and MVK concentrations significantly higher than those observed (by factors of ca. 2.5), indicating the possibility that isoprene chemistry is not effective for long enough for the secondary products to reach daytime quasi-steady-state concentration levels. To avoid such overestimation of secondary products from isoprene oxidation, isoprene was introduced only for a short time period (12 min) at the end of the calculations for each time of day. This treatment corresponds to a Lagrangian view that the air mass traveling to the site is influenced by isoprene chemistry for 12 min just before its arrival. The 12-min period was optimized such that the observed sum concentrations of MACR and MVK are reproduced (see Fig. S2): with isoprene oxidation durations of 10, 12, and 20 min, calculated MACR + MVK concentrations varied from 97 % to 115 % and 183 % of observations as midday (09:00–15:00 UTC) averages over the three days for the chemical mechanism of the base run. The same values were 89 %, 107 %, and 175 % for the chemical mechanism of run S1. The 12-min period is in rough agreement with the traveling time for the

ACPD
11, 28851–28894, 2011

air mass required to pass over the adjacent forest area (fetch is about 1 km), present in the upwind direction and deemed as the major source of isoprene, at a typical wind speed of about 2 m s^{-1}. Komenda et al. (2003) and Ammann et al. (2004) also suggested the importance of local emission for isoprene on the same campus. It should be noted that in all model runs discussed below, MVK and MACR were constrained by measurements and the 12-min period served to avoid buildup of excessive levels of unmeasured isoprene oxidation products in the model.

During nine 10-min periods, when valid NO measurements were not available or one standard deviation (calculated on the basis of raw data at ca. 100-s frequencies) exceeded the averages, the model results were not used in further analyses.

Table 2 summarizes the model runs made in this study. The outline of the base run was described above. Monte-Carlo simulations for the base run, where the uncertainty ranges of the reaction rate coefficients and of ancillary observations were taken into account (Tables S2 and S3; the values were taken from Sander et al. (2003) and Kanaya et al. (2007a) or determined from typical instrumental uncertainties and temporal variations), yielded total uncertainties (1σ) for the OH and HO_2 concentrations and HO_2/OH ratios of 28 %, 32 %, and 19 % for the noontime of 9 July and 17 %, 16 %, and 17 % for the noontime of 10 July, respectively.

Runs S1 and S2 take isomerization of isoprene peroxy radicals into account at rates proposed by Peeters and Müller (2010). This allowed formation of unsaturated hydroperoxy aldehydes, HPALD1 and HPALD2, whose photolysis frequencies were assumed to depend on the solar zenith angle, similar to the dependence of MACR, and the maximum value (with overhead sun) was assumed to be 5×10^{-4} s^{-1}, as suggested by Peeters and Müller (2010). The photolysis of HPALD1 and HPALD2 gave three OH molecules in the S1 run, and one OH molecule in the S2 run. Monte-Carlo simulations for these mechanisms using the parameters listed in Tables S2 and S3 yielded total uncertainties (1σ) for the OH and HO_2 concentrations and HO_2/OH ratios of 17 %, 16 %, and 17 % for both the S1 and the S2 run for the noontime of 10 July, respectively.

ACPD
11, 28851–28894, 2011

Another set of model runs was made as a variant of the base run and the S1 run, taking into account the missing OH reactivity. Five sensitivity model runs (Base_a(HC8), Base_b(XYL), Base_c(API), Base_d(OLI), and Base_e(mix)) were made as variants of the base run, where the missing reactivity was explained by additional HC8 (reactive alkanes with OH rate constants greater than 6.8×10^{-12} cm^3 s^{-1} for case Base_a(HC8)), XYL (xylene and more reactive aromatics for case Base_b(XYL)), API (pinenes for case Base_c(API)), OLI (internal olefins for case Base_d(OLI)), and their mixtures (32 % each from HC8, XYL, API, and OLI, and 4 % from OLI for case Base_e(mix)), respectively. The contributions from different types of hydrocarbons in the Base_e(mix) run were only determined arbitrarily. The S1 run was modified in that the missing OH reactivity was explained by additional HC8 (called the S1_a(HC8) run); this effectively impeded strong amplification of the radical chain reactions introduced by the isomerization of isoprene peroxy radicals.

As shown in Table 2, two more model runs (Base_e(mix)_HO_2_loss and S1_a(HC8)_HO_2_loss) were executed by incorporating loss terms for HO_2 with adjusted rates and OH yields, such that the observations were well reproduced by modeled OH, HO_2(*), and OH reactivities. Here, HO_2(*) is the value taking into account the sensitivity toward speciated RO_2 radicals, as found with the FZJ instrument in the HO_2 measurement mode (Fuchs et al., 2011).

4 Results and discussion

4.1 Comparisons with base run

Figure 2a,b shows time series of observed and modeled OH and HO_2 concentrations. It should be noted here again that RO_2 interferences in the HO_2 observation are not taken into account in this section, and will be analyzed in Sect. 4.5. In the base run, the features of the temporal variations of both OH and HO_2 are captured quite well by the model simulations. The order of the general magnitudes of the relationships was

ACPD
11, 28851–28894, 2011

MPI > base run > FRCGC > FZJ > DWD for OH, and MPI > base > FRCGC > FZJ for HO_2. Figure 2c shows the HO_2/OH ratios. The daytime HO_2/OH ratios from FRCGC and FZJ (especially on 9 and 10 July, before attachment of the RO_x converter (see Fuchs et al. (2010) for details) were well reproduced by the base model run. The MPI ratios on the three days (especially in the mornings) and the FZJ ratios on the morning of 11 July tended to be higher than the modeled values. Figure 3 (upper panels) shows scatterplots for observed and modeled OH and HO_2 concentrations and HO_2/OH ratios in the daytime period (06:00–18:00 UTC). Table 3 includes linear-regression parameters for these plots. All of the OH and HO_2 concentrations observed by the four instruments were fairly well reproduced by the base model run (slopes ranged from 0.81 to 1.33), with high R^2 values (0.72–0.97). The intercepts for OH and HO_2 ranged from -5.0 to 2.5×10^5 cm^{-3} and from -6.3 to -1.8×10^7 cm^{-3}, respectively. They are considered to be negligible when the uncertainties of the model calculation and observations are taken into account.

The result of our model-measurement comparison is surprisingly different from the findings of other campaigns which reported strong underprediction of observed OH levels at high VOC and low NO_x conditions. Here, we find that the base model reproduces the measured OH at HO_xComp fairly well to within 33 % over a range of 0.3–2 ppb isoprene and at NO mixing ratios as low as 0.1 ppb. At similar mixing ratios of isoprene and NO, observed OH was underpredicted by a box model by up to a factor of 8 in PRD (Hofzumahaus et al., 2009; Lu et al., 2011). At even lower NO (< 0.1 ppb) and in the presence of a few ppb isoprene, measured-to-modeled OH ratios reached even values up to ten in the rain forest in Suriname (Lelieveld et al., 2008) and Borneo (Whalley et al., 2011). In order to explain these large model-measurement discrepancies, unknown radical recycling reactions were postulated as additional OH source (Lelieveld et al., 2008; Hofzumahaus et al., 2009; Whalley et al., 2011). Apparently, such processes do not seem to play an important role for HO_xComp, or were possibly masked by other effects.

ACPD
11, 28851–28894, 2011

4.2 Comparisons with sensitivity runs (S1 and S2)

Next, we study the effects of the revised isoprene chemistry, postulated by Peeters and Müller (2010) to explain the missing OH source in forest environments. The results for HO_xComp are shown in the same figures as the base run (Figs. 2 and 3). The isoprene-chemistry revision increased OH and HO_2 concentrations as expected, by 43 % and 48 % on average for daytime (06:00–18:00 UTC), with respect to the base run results. The results from the S2 run are closer to those from the S1 run than to those from the base run. Averaged HPALD1 and HPALD2 concentrations in the afternoons (12:00–15:00 UTC) of 10 and 11 July, when isoprene concentrations were high, were 131 ppt (HPALD1) and 75 ppt (HPALD2) for the S1 run, and 123 ppt (HPALD1) and 71 ppt (HPALD2) for the S2 run. The OH yield of unity from the photolysis of HPALDs, as assumed in the S2 run, is effective in raising the OH and HO_2 concentrations significantly.

The OH and HO_2 concentrations in the S1 and S2 runs were significantly higher than those derived from the observations by DWD, FRCGC, and FZJ, at least at noon of 10 July, for which the model's uncertainties were calculated on the basis of a Monte-Carlo approach, but they were in reasonable agreement with the MPI observations. Figure 3 and Table 3 show that the results from the S1 run were more than 60 % higher than OH and HO_2 measured by DWD, FRCGC, and FZJ, although they were only 15 % and 21 % higher than the observations made by MPI. The regression lines for the HO_2/OH ratios with respect to the MPI data had significant negative intercept values (typically −50) in comparison with both the base and S1 runs. The RO_2 interference with the MPI instrument in the HO_2 measurements might be related to this. Table 3 also includes linear-regression parameters for the S2 run, with which the MPI data showed the best agreement (the slopes are 1.01 and 1.11 for OH and HO_2, respectively), but with a somewhat large HO_2 intercept (-1.1×10^8 cm^{-3}). For OH and HO_2 measurements by DWD, FRCGC, and FZJ, the slopes for the S1 and S2 runs cannot be explained by the combined 1σ uncertainties of observations and model calculations.

ACPD
11, 28851–28894, 2011

It is interesting to note that it was the same MPI instrument that flew over Suriname (with high isoprene concentrations) that measured OH and HO_2 concentrations higher than those modeled, for which the isomerization mechanism was proposed as an explanation. The HO_xComp observations made by the other instruments do not necessarily support the isomerization of isoprene peroxy radicals at the rates proposed by Peeters and Müller (2010). It should also be pointed out that the same FZJ instrument (which seems not to support the isomerization mechanism at HO_xComp) was used in PRD, where additional HO_x recycling was postulated to explain the HO_x observations (Hofzumahaus et al., 2009; Lu et al., 2011). Our finding from the HO_xComp campaign using observation ensembles is consistent with a recent laboratory study (Crounse et al., 2011) suggesting that the isomerization of isoprene peroxy radicals does take place, but at slower rates.

The degree of agreement between the FRCGC results and the base model run is better than in past studies using the same instruments and the standard RACM model calculations. The model tended to overestimate HO_2 concentrations by 44–89 % at coastal sites (except Okinawa Island), with R^2 values ranging between 0.34 and 0.79 (Kanaya and Akimoto, 2002). In Rishiri Island, the calculated/observed ratios for OH and HO_2 were 1.35 and 1.89, with R^2 values of 0.76 and 0.67 (Kanaya et al., 2007a). In Central Tokyo, the calculated/observed ratios for OH and HO_2 were 0.86 and 1.29 in the summer, with R^2 values of 0.41 and 0.85 (Kanaya et al., 2007b).

4.3 Radical production and loss processes

Figure 4 shows the breakdown of the radical production and radical loss processes for the base and S1 runs. They are separately shown as 3-h averages (09:00–12:00 and 12:00–15:00 UTC) on the three days. In the base run, HO_2 production is contributed mainly by the isoprene peroxy radical (ISOPBO2, ISOPDO2, ISOPEO2) +NO, OH + CO, CH_3O_2 + NO, HCHO + OH, and HCHO + *hν* reactions. HO_2 loss is dominated by reaction with NO. OH production is largely from the HO_2 + NO reaction. OH loss

ACPD
11, 28851–28894, 2011

is dominated by reactions with isoprene (especially in the afternoon), CO, and NO_2 (larger contributions in the morning). The major radical initiation sources for the radical group ($OH + HO_2 + RO_2$) are $O(^1D) + H_2O$, $HONO + h\nu$, and $HCHO + h\nu$. Terminal radical loss is mainly from $OH + NO_2$, but reactions of isoprene peroxy radicals with HO_2 and the HO_2 recombination reactions largely contributed in the afternoon of 10 July. For S1, isomerization of isoprene peroxy radicals and photolysis of HPALD1 and HPALD2 became important for individual and total radical production. The loss processes are not much different from those in the base run, but the $HO_2 + HO_2$ reaction became more important because of the larger HO_2 concentrations in the S1 run.

The gross OH production rates in S1 in the period 12:00–15:00 UTC on 10 and 11 July (6.0×10^7 and 6.1×10^7 radicals $cm^{-3}\,s^{-1}$, respectively) were 61 % and 38 % higher than those in the base run (3.7×10^7 and 4.4×10^7 radicals $cm^{-3}\,s^{-1}$, respectively); regeneration of OH radicals was enhanced by isomerization of isoprene peroxy radicals. The total radical ($OH + HO_2 + RO_2$) initiation rates for S1 in the same periods (2.5×10^7 and 1.8×10^7 radicals $cm^{-3}\,s^{-1}$, respectively) were 52 % and 34 % higher than those in the base run (1.6×10^7 and 1.4×10^7 radicals $cm^{-3}\,s^{-1}$, respectively).

Figure 5 shows the breakdown of peroxy radicals (HO_2 and RO_2) in the base and S1 runs. The major organic peroxy radicals are MO2 (CH_3O_2), isoprene peroxy radicals (ISOPBO2 + ISOPDO2 + ISOPEO2), saturated acylperoxy radicals (ACO3), and those from terminal olefins (OLTP). OLND and OLNN, formed from NO_3 reactions, dominated in the nighttime. It is interesting to note that the total peroxy radical concentrations in the base and S1 runs are not much different, but the fractions of HO_2 and isoprene peroxy radicals are larger and smaller, respectively, in the S1 run.

4.4 Comparisons with additional model runs satisfying observed levels of OH reactivity

In Fig. 6, the OH reactivities observed by the Tokyo Metropolitan University group are compared with the sum of the OH reaction rates with respect to each chemical species, including those measured and others (e.g., unmeasured secondary species) calculated

ACPD
11, 28851–28894, 2011

in the base run. Comparison between (A) and (C) in Fig. 6 indicated that the sum reactivity in the base model run is mainly contributed by reactions with observed species (including methane), rather than those with unmeasured secondary species calculated in the model. The agreement between the observed (B) and calculated (A) reactivities was very good on the morning of 9 July, when the NO_x concentrations were high, but differences were noticeable in the afternoon, typically 1.6 s^{-1}. Similar disagreements of about 2.5 s^{-1} were found in the morning and afternoon of 10 July. Although the observational data were limited, the magnitude of the difference was also similar in the afternoon of 11 July. Although some part of the discrepancy may be explained by uncertainties of observations and reaction rate coefficients, here we study several cases where this difference is explained by adding selected types of hydrocarbons in additional model runs. When reactivity observations were not available, the missing reactivities were estimated as the average before and after the period. The missing reactivities were assumed to be 0 and 3 s^{-1} before 05:00 UTC on 9 July and after 14:30 UTC on 11 July, respectively. In the case of the S1_a(HC8) run, the missing reactivity was recalculated as the difference between observation (when available) and the sum of the reactivities in the S1 model run; this was essentially the same as the results shown in Fig. 6.

In all cases except HC8 addition, not only the added hydrocarbon but also its secondary species non-negligibly contributed to the increase in the reactivity. The added amounts of hydrocarbons were adjusted such that the final model results gave OH reactivities consistent with observations to within 6 %. The mean differences in the reactivity (observation – model), about 1.7 s^{-1} in the base and S1 runs, became about $-0.3\,s^{-1}$ in the Base_e(mix) and S1_a(HC8) runs (Table 3). The daytime averages of the hydrocarbon concentrations assumed in the model runs were 9.4 ppb of HC8 (in the Base_a(HC8) run), 2.1 ppb of XYL (in the Base_b(XYL) run), 1.7 ppb of API (in the Base_ c(API) run), and 1.4 ppb of OLI (in the Base_d(OLI) run). In the Base_e(mix) run, the daytime averages were 3.1 ppb, 0.74 ppb, 0.54 ppb, and 0.13 ppb for HC8, XYL, API, and OLI, respectively. These concentrations are basically much larger than

ACPD
11, 28851–28894, 2011

those assumed in the base run (0.59 ppb of HC8, 0.10 ppb of XYL, 0.081 ppb of OLI, and 0 ppb of API). It is not very likely that a single class of hydrocarbons is present at such high concentrations; however, the possibility of the presence of multiple classes of hydrocarbons at smaller concentrations (e.g., Base_ e(mix) run) would be higher. For example, monoterpenes have previously been detected at levels of 0.1–0.5 ppb in the forest near the HO_xComp measurement site (Spirig et al., 2005), but were not measured during HO_xComp.

Figure 7a,b shows that the addition of HC8 (Base_a(HC8)) reduced OH and HO_2 concentrations, but the other runs adding a single class of hydrocabons, especially when adding XYL and OLI, resulted in effective radical-chain amplification, and thus higher HO_x concentrations. In the Base_b(XYL) run, secondary species such as methyl glyoxal (MGLY) and dicarbonyls (DCB) became important, whose photolysis produced radicals effectively. In the Base_c(OLI) run, ozonolysis of added olefins also contributed to the amplification. Although S1 resulted in OH and HO_2 levels that were too high compared with the results obtained from DWD/FRCGC/FZJ_HO_x, addition of HC8 in the S1_a(HC8) run brought the HO_x levels back to the levels of the base run (Fig. 7d,e).

Table 3 summarizes the bivariate regression parameters for the Base_e(mix) and S1_a(HC8) runs. For the Base_e(mix) run, the range of the slopes for OH and HO_2 was almost unchanged from those with the base run, except for HO_2_FZJ. However, the HO_2/OH ratios became significantly higher than the observed ratios (with slopes > 1.5, see also Fig. 7c). The Base_e(mix) run normally had lower R^2 values than those of the base run, except for those for the HO_2/OH ratios obtained by FZJ and MPI. The S1_a(HC8) run resulted in slopes nearer to unity for OH and HO_2 levels from DWD, FRCGC, and FZJ, than those obtained for the S1 run, but the HO_2/OH ratios were always higher than observed (with slopes > 1.4, see also Fig. 7f). In summary, isomerization of isoprene peroxy radicals at the rates proposed by Peeters and Müller (2010) could not be fully rejected because of the possible presence of unmeasured hydrocarbons (such as HC8) that could impede HO_x radical propagation.

ACPD
11, 28851–28894, 2011

4.5 RO_2 interference in HO_2 observations

Very recently, Fuchs et al. (2011) showed that HO_2 measurements by the FZJ instrument had large sensitivities toward organic peroxy radicals, such as those formed from isoprene, olefins, including MACR and MVK, and aromatic compounds. The MPI instrument has a similar degree of interference (Dillon, 2011) and it is possible that it occurs also with the FRCGC instrument, which used the same conversion process of HO_2 to OH (reaction with added NO) and achieved high conversion efficiencies, similar to those obtained by the FZJ instrument. However, this has not yet been fully characterized with the MPI and FRCGC instruments. In this section, the HO_2 levels observed by FZJ are compared with the modeled values, taking into account the sensitivity toward speciated RO_2 radicals, to see how the degree of agreement changes. The following RO_2 radicals were taken into account with relative sensitivities specified in parentheses (Fuchs et al., 2011; Lu et al., 2011): ETEP (0.85), OLTP (0.95), OLIP (0.95), isoprene peroxy radicals (ISOP or ISOPBO2, ISOPDO2, and ISOPEO2) (0.79), TOLP (0.86), XYLP (0.86), CSLP (0.86), and MACP (0.58). Here HO_2(*) represents the sum of the modeled HO_2 and the interference from modeled RO_2 weighted by the relative detection sensitivities. ETEP, OLIP, TOLP, XYLP, CSLP, and MACP are peroxy radicals formed from ethene, OLI, toluene and less reactive aromatics, XYL, hydroxyl substituted aromatics, and MACR, respectively. In the base and S1 runs, HO_2(*) were 42 % and 17 % larger than HO_2 on average. The smaller degree of increase in the S1 run is explained by the relatively lower abundance of RO_2 (see Fig. 5b). The modeled HO_2 concentrations and HO_2/OH ratios with and without RO_2 interference are compared with observations in Fig. 8. The regression parameters are also included in Table 3. In the base run, the slopes for the HO_2(*) concentration and the HO_2(*)/OH ratio (with RO_2 interference) became as high as 1.93 and 1.72, respectively, with similar R^2 values (Table 3). The significant overprediction for HO_2(*) by the model was evident for S1 (with a slope of 2.34), although the HO_2(*)/OH ratio was not significantly overestimated. For the Base_e(mix) run, where HO_2 (and RO_2) were even higher than in

ACPD
11, 28851–28894, 2011

the base run, the overestimation of HO_2(*) and HO_2(*)/OH became even worse (slopes were 2.49 and 2.12). In the S1_a(HC8) run, where radical concentrations were lower than those in the S1 run, the degree of overestimation was still significant (slopes were 1.84 and 1.64 for HO_2(*) and HO_2(*)/OH, respectively). The large deviations of the slopes from unity cannot be resolved by the model's uncertainty. These results strongly indicate that more loss processes for HO_2 (or interfering RO_2) will be necessary to explain these observations. This agrees with the findings by Whalley et al. (2011) and Lu et al. (2011) who concluded that the introduction of the isoprene isomerization mechanism by Peeters and Müller (2010) leads to an overprediction of observed HO_2 or HO_2(*) concentrations.

We tried re-modifications of the Base_e(mix) and the S1_a(HC8) model runs by including hypothetical HO_2-loss processes, such that all of the modeled OH, HO_2(*), and HO_2(*)/OH ratios reproduce observations simultaneously. In the Base_e(mix)_HO_2_loss run, we found that an additional reaction, $HO_2 \rightarrow 0.75\,OH$, at a constant rate of $0.2\,s^{-1}$ could bring OH, HO_2(*), and the HO_2(*)/OH ratio into agreement with the observations (see Fig. S3); the slopes of the regression lines were 0.96, 1.29, and 0.88, respectively, with high R^2values, 0.81–0.93 (Table 3). This additional process might be explained by combination of two processes, $HO_2 \rightarrow OH$ at a constant rate of $0.15\,s^{-1}$ and $HO_2 \rightarrow$ no products at a constant rate of $0.05\,s^{-1}$. The rate of HO_2-to-OH conversion ($0.15\,s^{-1}$) corresponds to an equivalent NO of 800 ppt. This is much smaller than the 1–7 ppb of equivalent NO required to bring afternoon OH and HO_2(*) levels into agreement with observations in PRD (model M2 in Lu et al., 2011). However, it is hard to suggest any potential processes that could explain this additional conversion. The rates of HO_2 loss with no product ($0.05\,s^{-1}$) are also significant, but might be partially explained by heterogeneous loss of HO_2 on aerosol surfaces, whose rates at upper limits have been estimated to be $0.1\,s^{-1}$ for PRD (Lu et al., 2011) and $0.04\,s^{-1}$ for Tokyo (Kanaya et al., 2007b), using a high uptake coefficient ($\gamma \geq 0.5$).

In the S1_a(HC8)_HO_2_loss run, we found that an additional reaction, $HO_2 \rightarrow 0.7OH$ at a slower rate of $0.04\,s^{-1}$, could bring daytime OH, HO_2(*), and the HO_2(*)/OH ratio

ACPD
11, 28851–28894, 2011

into agreement with observations (see Fig. S3). Again, the identification of the processes is currently infeasible. It should be noted that these rates and OH yields are not derived as unique solutions; there can be another combination of the parameters that could explain the observations. Here, we only aimed at crude estimations of these parameters.

From the budget analysis of the radicals in these two runs (Fig. S4), sometimes up to several tens of percents of HO_2 loss, OH production, and radical loss rates need to be explained by the hypothetical HO_2 reactions. Clearly, more studies are needed to explain these discrepancies. Also, RO_2 interference should be quantitatively studied with the FRCGC and MPI instruments.

4.6 Behavior on the morning of 9 July: model's underestimation of HO_2 at high NO

Because of the good agreement between observed and simulated OH reactivities and the low isoprene concentrations, the morning of 9 July was deemed to be an ideal period, where all model results tended to converge. Here, the observation ranges are compared to the full range from the model ensemble runs mentioned above (except runs with hypothetical HO_2-loss processes) and to the uncertainty range of the base run (Fig. 9). The observed OH concentrations from all groups fall within the full range of the model ensemble runs and within the uncertainty range of the base run, except for some high points for FRCGC and FZJ, usually associated with large fluctuations during the 10-min periods (Fig. 9a). The DWD_OH data were slightly lower than the ranges; the observational accuracy could explain these differences. On the other hand, the HO_2 concentrations and the HO_2/OH ratios from MPI were higher than those from the model results (Fig. 9b). The same but weaker tendencies were, in general, present for FRCGC and FZJ. Several HO_2/OH ratios from FRCGC were also high, but these were normally associated with large fluctuations during the 10-min periods (Fig. 9c). The large model-to-observation discrepancies found for this period would most likely be attributable to the possibility of unknown chemistry or to measurement issues. One

ACPD
11, 28851–28894, 2011

possibility with respect to measurement issues is that RO_2 radicals are interfering with the HO_2 observations. However, modeled HO_2(*) levels for the FZJ instruments are still lower than the FZJ observations (Fig. 9d). Thus, in the following paragraphs, the possibility of unknown chemistry is discussed.

The morning period on 9 July was associated with relatively high NO_x concentrations. In Fig. 10b, where modeled-to-observed HO_2 ratios in the daytime (06:00–18:00 UTC) are plotted against NO concentrations, this underestimation by the model is evident only under the high NO conditions seen on the morning of 9 July. This tendency is opposite to the normal low NO cases, where general features were weak overestimations of HO_2 (for FRCGC and FZJ), as discussed in the previous sections. The changes in the ratios are smooth against NO. Such a tendency has been discussed before, by Martinez et al. (2003) for Nashville, Ren et al. (2003, 2006) for New York, and Kanaya et al. (2007b) for Tokyo, using a single instrument for each experiment. HO_xComp provided an opportunity to verify this tendency with three instruments being operated simultaneously, for the first time. The same tendency was present for the ratio with modeled HO_2(*), but this is not shown. It is interesting to note that the same tendency is also clear, if the ratio of modeled to observed HO_2 is plotted against NO_2 and NO_x (Fig. 10d), although this was unclear in Tokyo (Kanaya et al., 2007b).

We previously proposed processes that could explain these results (Kanaya et al., 2007b), including (1) HNO_4 reactions, such as reaction with NO producing two HO_2 molecules, and (2) missing HO_x production, with a rate proportional to the NO concentration. An additional HO_xComp model run with hypothetical HO_2 production of strength (NO (cm^{-3})) $\times 5 \times 10^{-5}$ (radicals $cm^{-3}\,s^{-1}$) countered the trend of the modeled-to-observed HO_2 against NO (not shown). The factor of 5×10^{-5} was larger than that of 2×10^{-5}, which effectively countered the trend in Tokyo (Kanaya et al., 2007b). This trend is very important in the ozone production regime. In Fig. 11, the dependences of the $HO_2 + NO$ reaction rates for the midday period (09:00–15:00 UTC) on NO concentrations are shown individually for the values derived from HO_2 observed by the FRCGC instrument and for HO_2 modeled by the base run. This reaction normally

ACPD
11, 28851–28894, 2011

governs the ozone production. The modeled rate has a maximum at NO mixing ratios of around 1 ppbv, and then shows saturation with further increases in NO. This saturation corresponds to the "NO_x-saturated" behavior of ozone production at high NO_x. In contrast, the rate using observed HO_2 concentrations monotonously increased with NO, resulting in a permanent NO_x-limited feature. Further studies of the HO_2 behavior at high NO_x conditions in the field and in the laboratory (including chamber studies) are highly recommended.

Figure 10a,c also shows that model/observation ratios for OH are almost flat throughout the NO (and NO_x) concentration ranges. This is clearly different from the behavior found in PRD, where the observation/model ratios were >2.5 at NO concentrations of 0.3 ppb (Lu et al., 2011). The different behavior at HO_xComp may be related to the lower isoprene and VOC reactivity or the short time exposure of isoprene to OH. Further studies are also required to explain this difference found for OH.

5 Summary

Daytime OH and HO_2 concentrations and HO_2/OH ratios in ambient air were observed by multiple instruments for three days of the HO_xComp field campaign held in Jülich, Germany, in July 2005. The concentrations were compared with box-model simulations using different assumptions for isoprene chemistry and for additional hydrocarbons to explain the observed OH reactivity. The agreement with the base run was remarkable, suggesting that HO_xComp did not need additional radical recycling to explain OH in the presence of isoprene at low NO, as opposed to the cases for the measurements in Suriname (Kubistin et al., 2010) and PRD (Hofzumahaus et al., 2009; Lu et al., 2011). An important difference in the chemical conditions at HO_xComp is the fact that the measurement site experienced fresh isoprene emissions that were only a little photochemically aged. This may be an indication that the unexplained large OH concentrations in Amazonia and PRD were caused by second- or third-generation products from VOC oxidations.

ACPD
11, 28851–28894, 2011

Introducing isomerization of isoprene peroxy radicals incurred overprediction by the model of radical concentrations with respect to OH and HO_2 observed by a CIMS instrument and two LIF instruments. However, the degree of overestimation could be diminished for OH when reactive alkanes (HC8) were solely introduced to the model to explain the missing fraction of observed OH reactivity. The isomerization of isoprene peroxy radicals at the rates proposed by Peeters and Müller (2010) was therefore regarded as unlikely, but was not fully rejected. It is further noted that the overprediction of the measured HO_2 or HO_2(*) levels by the isoprene isomerization scheme is similar to the findings by Lu et al. (2011) and Whalley et al. (2011) at PRD and Borneo, respectively.

The large sensitivity toward various RO_2 species in the FZJ-LIF instrument in the HO_2 measurement mode perturbed the relatively good agreement between the observations and the aforementioned model runs, requiring strong unknown loss processes for HO_2.

On the morning of 9 July, regarded as an ideal case because the OH reactivity was well explained and isoprene concentrations were low, we found a tendency for the models to underestimate HO_2, the opposite of the normal tendency of weak overestimation for HO_2. The underestimation, commonly found for the three LIF measurements, was associated with high NO conditions and was not explained by RO_2 interference. One possibility is that a missing HO_x source or regeneration process becomes important under these conditions, and this could influence our understanding of ozone production regimes.

Supplementary material related to this article is available online at: http://www.atmos-chem-phys-discuss.net/11/28851/2011/acpd-11-28851-2011-supplement.pdf.

ACPD
11, 28851–28894, 2011

Acknowledgements. This work was supported by the EU FP-6 program EUROCHAMP (grant no. RII3-CT-2004-505968), ACCENT (Priority 1.1.6.3. *Global Change and Ecosystems*, grant no. GOCE-CT-2004-505337), a Grant-in-Aid for Scientific Research (KAKENHI) (B) 22310018 and RR2002 of the Kyosei Project by the Ministry of Education, Science, Sports, and Culture of Japan. We thank F. J. Johnen for assistance with the experiments and K. D. Lu for discussions.

References

Ammann, C., Spirig, C., Neftel, A., Steinbacher, M., Komenda, M., and Schaub, A.: Application of PTR-MS for measurements of biogenic VOC in a deciduous forest, Int. J. Mass Spectrom., 239, 87–101, 2004.

Archibald, A. T., Cooke, M. C., Utembe, S. R., Shallcross, D. E., Derwent, R. G., and Jenkin, M. E.: Impacts of mechanistic changes on HO_x formation and recycling in the oxidation of isoprene, Atmos. Chem. Phys., 10, 8097–8118, doi:10.5194/acp-10-8097-2010, 2010.

Berresheim, H., Elste, T., Plass-Dülmer, C., Eisele, F. L., and Tanner, D. J.: Chemical ionization mass spectrometer for long-term measurements of atmospheric OH and H_2SO_4, Int. J. Mass Spectrom., 202, 91–109, doi:10.1016/S1387-3806(00)00233-5, 2000.

Brasseur, G., Hauglustaine, D., Walters, S., Rasch, R., Müller, J.-F., Granier, C., and Tie, X.: MOZART, a global chemical transport model for ozone and related chemical tracers 1. Model description, J. Geophys. Res., 103, 28265–28289, 1998.

Crounse, J. D., Paulot, F., Kjaergaard, H. G., and Wennberg, P. O.: Peroxy radical isomerization in the oxidation of isoprene, Phys. Chem. Chem. Phys., 13, 13607–13613, doi:10.1039/C1CP21330J, 2011.

Di Carlo, P., Brune, W. H., Martinez, M., Harder, H., Lesher, R., Ren, X., Thornberry, T., Carroll, M. A., Young, V., Shepson, P. B., Riemer, D., Apel, E., and Campbell, C.: Missing OH reactivity in a forest: evidence for unknown reactive biogenic VOCs, Science, 304, 722–725, 2004.

Dillon, T. J.: Interactive comment on "Detection of HO_2 by laser-induced fluorescence: calibration and interferences from RO_2 radicals" by H. Fuchs et al., Atmos. Meas. Tech. Discuss., 4, C210–C213, 2011.

Dillon, T. J. and Crowley, J. N.: Direct detection of OH formation in the reactions of HO_2

ACPD

11, 28851–28894, 2011

with $CH_3C(O)O_2$ and other substituted peroxy radicals, Atmos. Chem. Phys., 8, 4877–4889, doi:10.5194/acp-8-4877-2008, 2008.

Fuchs, H., Brauers, T., Dorn, H.-P., Harder, H., Hseler, R., Hofzumahaus, A., Holland, F., Kanaya, Y., Kajii, Y., Kubistin, D., Lou, S., Martinez, M., Miyamoto, K., Nishida, S., Rudolf, M., Schlosser, E., Wahner, A., Yoshino, A., and Schurath, U.: Technical Note: Formal blind intercomparison of HO_2 measurements in the atmosphere simulation chamber SAPHIR during the HO_xComp campaign, Atmos. Chem. Phys., 10, 12233–12250, doi:10.5194/acp-10-12233-2010, 2010.

Fuchs, H., Bohn, B., Hofzumahaus, A., Holland, F., Lu, K. D., Nehr, S., Rohrer, F., and Wahner, A.: Detection of HO_2 by laser-induced fluorescence: calibration and interferences from RO_2 radicals, Atmos. Meas. Tech., 4, 1209–1225, doi:10.5194/amt-4-1209-2011, 2011.

Heland, J., Kleffmann, J., Kurtenbach, R., and Wiesen, P.: A new instrument to measure gaseous nitrous acid (HONO) in the atmosphere, Environ. Sci. Technol., 35, 3207–3212, 2001.

Hofzumahaus, A., Rohrer, F., Lu, K., Bohn, B., Brauers, T., Chang, C.-C., Fuchs, H., Holland, F., Kita, K., Kondo, Y., Li, X., Lou, S., Shao, M., Zeng, L., Wahner, A., and Zhang, Y.: Amplified trace gas removal in the troposphere, Science, 324, 1702–1704, 2009.

Kanaya, Y. and Akimoto, H.: Radicals in the marine boundary layer: testing the current tropospheric chemistry mechanism, Chem. Rec., 2, 199–211, 2002.

Kanaya, Y. and Akimoto, H.: Gating a channel photomultiplier using a fast high voltage switch: Reduction of afterpulse rates in a laser-induced fluorescence instrument for measurement of atmospheric OH radical concentrations, Appl. Opt., 45, 1254–1259, 2006.

Kanaya, Y., Sadanaga, Y., Hirokawa, Kajii, Y., and Akimoto, H.: Development of a ground-based LIF instrument for measuring HO_x radicals: instrumentation and calibrations, J. Atmos. Chem., 38, 73–110, doi:10.1023/A:1026559321911, 2001.

Kanaya, Y., Cao, R., Kato, S., Miyakawa, Y., Kajii, Y., Tanimoto, H., Yokouchi, Y., Mochida, M., Kawamura, K., and Akimoto, H.: Chemistry of OH and HO_2 radicals observed at Rishiri Island, Japan, in September 2003: missing daytime sink of HO_2 and positive nighttime correlations with monoterpenes, J. Geophys. Res., 112, D11308, doi:10.1029/2006JD007987, 2007a.

Kanaya, Y., Cao, R., Akimoto, H., Fukuda, M., Komazaki, Y., Yokouchi, Y., Koike, M., Tanimoto, H., Takegawa, N., and Kondo, Y.: Urban photochemistry in Central Tokyo: 1. Observed and modeled OH and HO_2 radical concentrations during the winter and summer of 2004, J.

ACPD

11, 28851–28894, 2011

Geophys. Res., 112, D21312, doi:10.1029/2007JD008670, 2007b.
Kleffmann, J., Gavriloaiei, T., Hofzumahaus, A., Holland, F., Koppmann, R., Rupp, L., Schlosser, E., Siese, M., and Wahner, A.: Daytime formation of nitrous acid: a major source of OH radicals in a forest, Geophys. Res. Lett., 32, L05818, doi:10.1029/2005GL022524, 2005.
Komenda, M., Schaub, A., and Koppmann, R.: Description and characterization of an on-line system for long-term measurements of isoprene, methyl vinyl ketone, and methacrolein in ambient air, J. Chromat. A, 995, 185–201, 2003.
Kubistin, D., Harder, H., Martinez, M., Rudolf, M., Sander, R., Bozem, H., Eerdekens, G., Fischer, H., Gurk, C., Klüpfel, T., Königstedt, R., Parchatka, U., Schiller, C. L., Stickler, A., Taraborrelli, D., Williams, J., and Lelieveld, J.: Hydroxyl radicals in the tropical troposphere over the Suriname rainforest: comparison of measurements with the box model MECCA, Atmos. Chem. Phys., 10, 9705–9728, doi:10.5194/acp-10-9705-2010, 2010.
Lelieveld, J., Butler, T. M., Crowley, J., Dillon, T., Fischer, H., Ganzeveld, L., Harder, H., Lawrence, M. G., Martinez, M., Taraborrelli, D., and Williams, J.: Atmospheric oxidation capacity sustained by a tropical forest, Nature, 452, 737–740, 2008.
Lu, K. D., Rohrer, F., Holland, F., Fuchs, H., Bohn, B., Brauers, T., Chang, C. C., Häseler, R., Hu, M., Kita, K., Kondo, Y., Li, X., Lou, S. R., Nehr, S., Shao, M., Zeng, L. M., Wahner, A., Zhang, Y. H., and Hofzumahaus, A.: Observation and modelling of OH and HO_2 concentrations in the Pearl River Delta 2006: a missing OH source in a VOC rich atmosphere, Atmos. Chem. Phys. Discuss., 11, 11311–11378, doi:10.5194/acpd-11-11311-2011, 2011.
Martinez, M., Harder, H., Kovacs, T. A., Simpas, J. B., Bassis, J., Lesher, R., Brune, W. H., Frost, G. J., Willians, E. J., Stroud, C. A., Jobson, B. T., Roberts, J. M., Hall, S. R., Shetter, R. E., Wert, B., Fried, A., Akicke, B., Stutz, J., Young, V. L., White, A. B., and Zamora, R. J.: OH and HO_2 concentrations, sources, and loss rates during the Southern Oxidants Study in Nashville, Tennessee, summer 1999, J. Geophys. Res., 108, 4617, doi:10.1029/2003JD003551, 2003.
Martinez, M., Harder, H., Kubistin, D., Rudolf, M., Bozem, H., Eerdekens, G., Fischer, H., Klüpfel, T., Gurk, C., Königstedt, R., Parchatka, U., Schiller, C. L., Stickler, A., Williams, J., and Lelieveld, J.: Hydroxyl radicals in the tropical troposphere over the Suriname rainforest: airborne measurements, Atmos. Chem. Phys., 10, 3759–3773, doi:10.5194/acp-10-3759-2010, 2010.
Paulot, F., Crounse, J. D., Kjaergaard, H. G., Kürten, A., St. Clair, J. M., Seinfeld, J. H., and

ACPD
11, 28851–28894, 2011

Wennberg, P. O.: Unexpected epoxide formation in the gas-phase photooxidation of isoprene, Science, 325, 730–733, 2009.
Peeters, J. and Müller, J.-F.: HO_x radical regeneration in isoprene oxidation via peroxy radical isomerisations, II: Experimental evidence and global impact, Phys. Chem. Chem. Phys., 12, 14227–14235, 2010.
Peeters, J., Nguyen, T. L., and Vereecken, L.: HO_x radical regeneration in the oxidation of isoprene, Phys. Chem. Chem. Phys., 11, 5935–5939, doi:10.1039/b908511d, 2009.
Pöschl, U., von Kuhlmann, R., Poisson, N., and Crutzen, P. J.: Development and intercomparison of condensed isoprene oxidation mechanisms for global atmospheric modeling, J. Atmos. Chem., 37, 29–52, 2000.
Pugh, T. A. M., MacKenzie, A. R., Hewitt, C. N., Langford, B., Edwards, P. M., Furneaux, K. L., Heard, D. E., Hopkins, J. R., Jones, C. E., Karunaharan, A., Lee, J., Mills, G., Misztal, P., Moller, S., Monks, P. S., and Whalley, L. K.: Simulating atmospheric composition over a South-East Asian tropical rainforest: performance of a chemistry box model, Atmos. Chem. Phys., 10, 279–298, doi:10.5194/acp-10-279-2010, 2010.
Ravishankara, A. R., Dunlea, E. J., Blitz, M. A., Dillon, T. J., Heard, D. E., Pilling, M. J., Strekowski, R. S., Nicovich, J. M., and Wine, P. H.: Redetermination of the rate coefficient for the reaction of $O(^1D)$ with N_2, Geophys. Res. Lett., 29, 1745, doi:10.1029/2002GL014850, 2002.
Ren, X., Harder, H., Martinez, M., Lesher, R. L., Oliger, A., Simpas, J. B., Brune, W. H., Schwab, J. J., Demerjian, K. L., He, Y., Xhou, X., and Gao, H.: OH and HO_2 chemistry in the urban atmosphere of New York City, Atmos. Environ., 37, 3639–3651, 2003.
Ren, X., Brune, W. H., Mao, J., Mitchell, M. J., Lesher, R. L., Simpas, J. B., Metcalf, A. R., Schwab, J. J., Cai, C., Li, Y., Demerjian, K. L., Felton, H. D., Boynton, G., Adams, A., Perry, J., He. Y., Zhou, X., and Hou, J.: Behavior of OH and HO_2 in the winter atmosphere in New York City, Atmos. Environ., 40, S252–S263, 2006.
Ren, X., Olson, J. R., Crawford, J. H., Brune, W. H., Mao, J., Long, R. B., Chen, Z., Chen, G., Avery, M. A., Sachse, G. W., Barrick, J. D., Diskin, G. S., Huey, L. G., Fried, A., Cohen, R. C., Heikes, B., Wennberg, P. O., Singh, H. B., Blake, D. R., and Shetter, R. E.: HO_x chemistry during INTEX-A 2004: Observation, model calculation, and comparison with previous studies, J. Geophys. Res., 113, D05310, doi:10.1029/2007JD009166, 2008.
Rohrer, F. and Berresheim, H.: Strong correlation between levels of tropospheric hydroxyl radicals and solar ultraviolet radiation, Nature, 442, 7099, 184–187, doi:10.1038/nature04924,

ACPD
11, 28851–28894, 2011

2006.
Sadanaga, Y., Yoshino, A., Kato, S., Kajii, Y.: Measurements of OH reactivity and photochemical ozone production in the urban atmosphere, Environ. Sci. Technol., 39, 8847–8852, 2005.
Sander, S. P., Friedl, R. R., Golden, D. M., Kurylo, M. J., Huie, R. E., Orkin, V. L., Mootgat, G. K., Ravishankara, A. R., Kolb, C. E., Molina, M. J., Finlayson-Pitts, B. J.: Chemical kinetics and photochemical data for use in stratospheric modeling, evaluation number 14, JPL Publ. 02–25, Natl. Aeronaut. Space Admin., Jet Propul. Lab., Pasadena, Calif, 2003.
Schlosser, E., Brauers, T., Dorn, H.-P., Fuchs, H., Häseler, R., Hofzumahaus, A., Holland, F., Wahner, A., Kanaya, Y., Kajii, Y., Miyamoto, K., Nishida, S., Watanabe, K., Yoshino, A., Kubistin, D., Martinez, M., Rudolf, M., Harder, H., Berresheim, H., Elste, T., Plass-Dülmer, C., Stange, G., and Schurath, U.: Technical Note: Formal blind intercomparison of OH measurements: results from the international campaign HO_xComp, Atmos. Chem. Phys., 9, 7923–7948, doi:10.5194/acp-9-7923-2009, 2009.
Sommariva, R., Haggerstone, A.-L., Carpenter, L. J., Carslaw, N., Creasey, D. J., Heard, D. E., Lee, J. D., Lewis, A. C., Pilling, M. J., and Zádor, J.: OH and HO_2 chemistry in clean marine air during SOAPEX-2, Atmos. Chem. Phys., 4, 839–856, doi:10.5194/acp-4-839-2004, 2004.
Spirig, C., Neftel, A., Ammann, C., Dommen, J., Grabmer, W., Thielmann, A., Schaub, A., Beauchamp, J., Wisthaler, A., and Hansel, A.: Eddy covariance flux measurements of biogenic VOCs during ECHO 2003 using proton transfer reaction mass spectrometry, Atmos. Chem. Phys., 5, 465–481, doi:10.5194/acp-5-465-2005, 2005.
Stavrakou, T., Peeters, J., and Müller, J.-F.: Improved global modelling of HO_x recycling in isoprene oxidation: evaluation against the GABRIEL and INTEX-A aircraft campaign measurements, Atmos. Chem. Phys., 10, 9863–9878, doi:10.5194/acp-10-9863-2010, 2010.
Stockwell, W. R., Kirchner, F., Kuhn, M., and Seefeld, S.: A new mechanism for regional atmospheric chemistry modeling, J. Geophys. Res., 102, 25847–25880, 1997.
Taraborrelli, D., Lawrence, M. G., Butler, T. M., Sander, R., and Lelieveld, J.: Mainz Isoprene Mechanism 2 (MIM2): an isoprene oxidation mechanism for regional and global atmospheric modelling, Atmos. Chem. Phys., 9, 2751–2777, doi:10.5194/acp-9-2751-2009, 2009.
Wennberg, P. O., Hanisco, T. F., Jaeglé, L., Jacob, D. J., Hintsa, E. J., Lanzendorf, E. J., Anderson, J. G., Gao, R.-S., Keim, E. R., Donnelly, S. G., Del Negro, L. A., Fahey, D. W., McKeen, S. A., Salawitch, R. J., Webster, C. R., May, R. D., Herman, R. L., Proffitt, M. H., Margitan, J. J., Atlas, E. L., Schauffler, S. M., Flocke, F., McElroy, C. T., and Bui, T. P.: Hydrogen radicals, nitrogen radicals, and the production of O_3 in the upper troposphere, Science,

ACPD
11, 28851–28894, 2011

279, 49–53, 1998.

Whalley, L. K., Edwards, P. M., Furneaux, K. L., Goddard, A., Ingham, T., Evans, M. J., Stone, D., Hopkins, J. R., Jones, C. E., Karunaharan, A., Lee, J. D., Lewis, A. C., Monks, P. S., Moller, S. J., and Heard, D. E.: Quantifying the magnitude of a missing hydroxyl radical source in a tropical rainforest, Atmos. Chem. Phys., 11, 7223–7233, doi:10.5194/acp-11-7223-2011, 2011.

Yoshino, A., Sadanaga, Y., Watanabe, K., Kato, S., Miyakawa, Y., Matsumoto, J., Kajii, Y.: Measurement of total OH reactivity by laser-induced pump and probe technique – comprehensive observations in the urban atmosphere of Tokyo, Atmos. Environ., 40, 7869–7881, 2006.

Zhang, L., Brook, J. R., and Vet, R.: A revised parameterization for gaseous dry deposition in air-quality models, Atmos. Chem. Phys., 3, 2067–2082, doi:10.5194/acp-3-2067-2003, 2003.

ACPD

11, 28851–28894, 2011

Table 1. Instruments measuring OH and HO_2 during the ambient measurement period of the HO_xComp campaign.

	OH accuracy (%) (1σ)	OH LOD (10^5 cm^{-3}) ($S/N = 2$)	Δt (s)	HO_2 accuracy (%) (1σ)[a]	HO_2 LOD (pptv) ($S/N = 2$)	Δt (s)
DWD_CIMS	19	4.5	8			
FRCGC_LIF	20	5.3	73	24	0.22	73
MPI_LIF	16	11	5	16	0.68	5
FZJ_LIF	10	4.9	137	10	0.86	30

[a] HO_2 accuracies do not include possible systematic errors due to interference by RO_2.

ACPD
11, 28851–28894, 2011

Table 2. Descriptions of model runs.

Name	Isomerization of isoprene peroxy radicals; photolysis of HPALDs	NMHC added to explain observed OH reactivity	Additional HO_2 loss
Base run	NO	NO	NO
S1	YES HPALD1 (HPALD2) + $h\nu \rightarrow$ 3OH	NO	NO
S2	YES HPALD1 (HPALD2) + $h\nu \rightarrow$ 1OH	NO	NO
Base_a (HC8)	NO	HC8	NO
Base_b (XYL)	NO	XYL	NO
Base_c (API)	NO	API	NO
Base_d (OLI)	NO	OLI	NO
Base_e (mix)	NO	32 % from HC8, XYL, and API and 4 % from OLI	NO
S1_a (HC8)	YES HPALD1 (HPALD2) + $h\nu \rightarrow$ 3OH	HC8	NO
Base_e(mix)_HO_2_loss	NO	32 % from HC8, XYL, and API and 4 % from OLI	$HO_2 \rightarrow 0.75$OH ($0.2\,s^{-1}$)
S1_a(HC8)_HO_2_loss	YES HPALD1 (HPALD2) + $h\nu \rightarrow$ 3OH	HC8	$HO_2 \rightarrow 0.7$OH ($0.04\,s^{-1}$)

ACPD
11, 28851–28894, 2011

Table 3. Linear-regression parameters for daytime (defined as 06:00–18:00 UTC). Slopes larger than unity indicate model overestimation. Intercepts are for the *y*-axis for model values.

	Base			S1			S2			Base_e(mix)			S1_a(HC8)			Base_e(mix)_HO_2 loss			S1_a(HC8)_HO_2 loss		
	slope	intercept	R^2	slope	intercept	R^2	slope	intercept	R^2	slope	intercept	R^2	slope	intercept	R^2	slope	intercept	R^2	slope	intercept	R^2
OH_DWD	1.33	2.5E+05	0.86	1.89	−5.7E+05	0.94	1.65	−1.9E+05	0.92	1.32	7.9E+05	0.69	1.06	3.6E+05	0.81						
OH_FRCGC	1.06	−4.4E+05	0.72	1.61	−2.0E+06	0.68	1.37	−1.3E+06	0.70	1.02	2.3E+05	0.66	0.82	−7.9E+04	0.71						
OH_FZJ	1.15	−5.0E+05	0.79	1.76	−2.1E+06	0.69	1.49	−1.4E+06	0.73	1.15	9.1E+02	0.73	0.91	−2.4E+05	0.79	0.96	2.7E+05	0.81	0.87	−2.6E+05	0.78
OH_MPI	0.81	1.7E+05	0.87	1.15	−6.3E+05	0.95	1.01	−2.6E+05	0.94	0.79	7.2E+05	0.71	0.65	2.6E+05	0.83						
HO_2_FRCGC	1.11	−1.8E+07	0.97	1.63	−5.1E+07	0.98	1.50	−4.4E+07	0.98	1.32	1.7E+07	0.93	1.24	−2.1E+07	0.97						
HO_2_FZJ	1.33	−3.8E+07	0.91	1.96	−8.5E+07	0.92	1.79	−7.3E+07	0.92	1.85	−2.9E+07	0.85	1.60	−5.5E+07	0.92	0.51	1.6E+07	0.64	0.99	−2.2E+07	0.90
HO_2_MPI	0.82	−6.3E+07	0.95	1.21	−1.2E+08	0.95	1.11	−1.1E+08	0.95	0.97	−2.9E+07	0.94	0.91	−7.2E+07	0.95						
HO_2/OH_FRCGC	1.15	−5.3E+00	0.90	1.07	−4.0E+00	0.90	1.13	−5.2E+00	0.90	1.57	−6.1E+00	0.90	1.49	−6.3E+00	0.88						
HO_2/OH_FZJ	1.14	−7.7E+00	0.78	1.06	−6.4E+00	0.78	1.12	−7.4E+00	0.78	1.52	−7.3E+00	0.82	1.43	−6.9E+00	0.81	0.25	1.0E+01	0.66	0.77	4.9E+00	0.79
HO_2/OH_MPI	1.72	−5.4E+01	0.86	1.63	−5.0E+01	0.86	1.70	−5.3E+01	0.86	2.38	−7.2E+01	0.88	2.30	−7.1E+01	0.87						
HO_2 (*)_FZJ	1.93	−6.5E+07	0.93	2.34	−9.6E+07	0.93	2.12	−8.1E+07	0.93	2.49	−4.8E+07	0.88	1.84	−6.1E+07	0.92	1.29	−2.1E+07	0.93	1.25	−3.1E+07	0.90
HO_2 (*)/OH_FZJ	1.72	−1.6E+01	0.79	1.28	−7.1E+00	0.80	1.33	−8.1E+00	0.80	2.12	−1.5E+01	0.83	1.64	−7.6E+00	0.82	0.88	3.1E+00	0.81	0.95	4.4E+00	0.81
OH reactivity mean bias (obs–model)		1.65			1.67			1.67			−0.29			−0.26			−0.17			−0.21	

Units for the intercept and OH reactivity are cm^{-3} and s^{-1}, respectively.
HO_2(*) indicates comparisons with modeled $HO_2 + RO_2$ artifacts. See text for details.

ACPD
11, 28851–28894, 2011

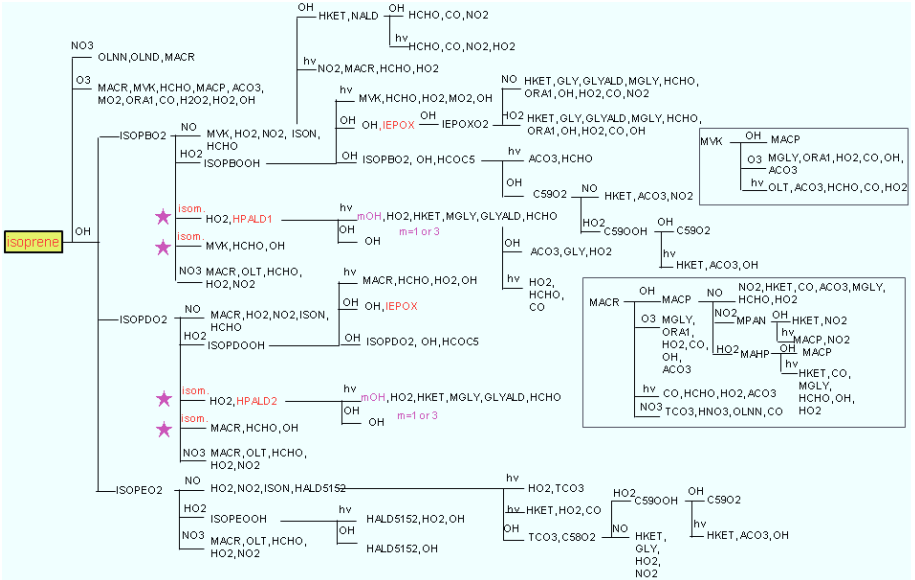

Fig. 1. Revised isoprene chemistry used in this study. The four processes with stars are isomerization reactions of isoprene peroxy radicals additionally taken into account in the S1, S2, S1_a(HC8), and S1_a(HC8)_HO_2_ loss model runs.

ACPD
11, 28851–28894, 2011

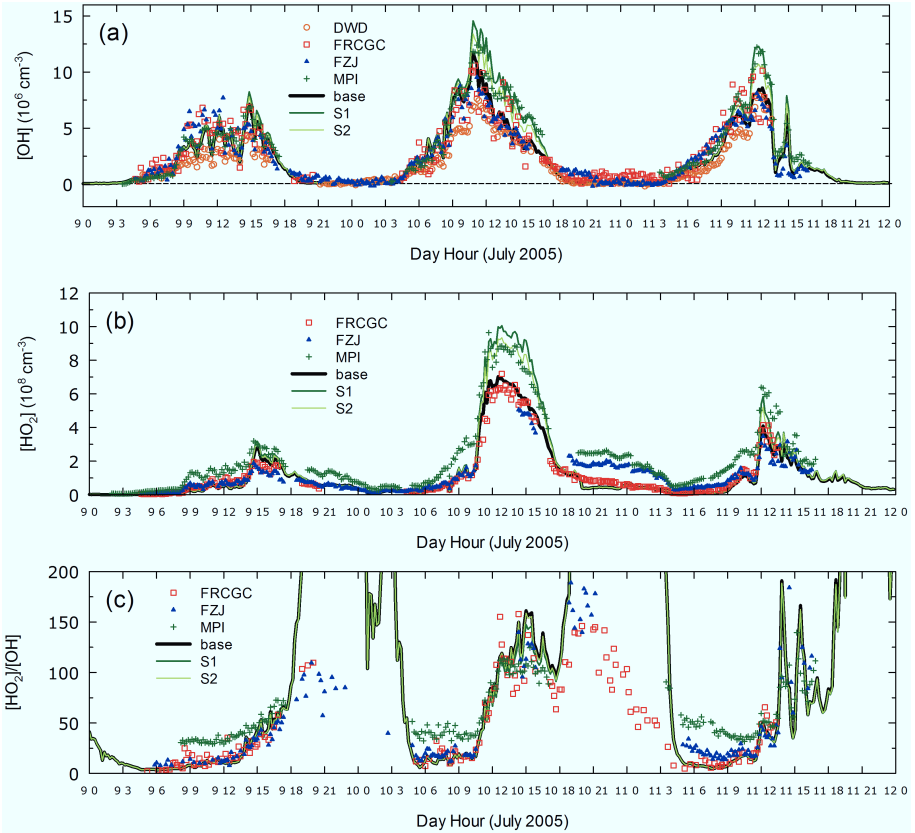

Fig. 2. Comparisons of observed and modeled **(a)** OH and **(b)** HO_2 concentrations, and **(c)** HO_2/OH ratios. The results from the base, S1, and S2 runs are shown. The HO_2/OH ratios in the base run and in the S1 run are in close match to those in the S2 run for most of the period.

ACPD
11, 28851–28894, 2011

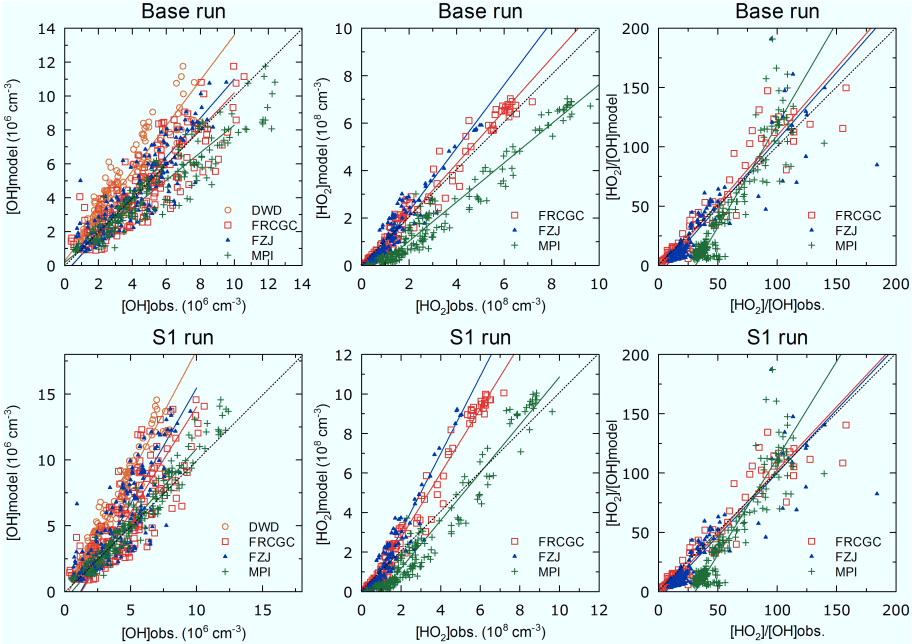

Fig. 3. Scatterplots between observed OH and HO_2 concentrations and HO_2/OH ratios, and those modeled in the base run (upper panels) and in the S1 run (lower panels).

ACPD
11, 28851–28894, 2011

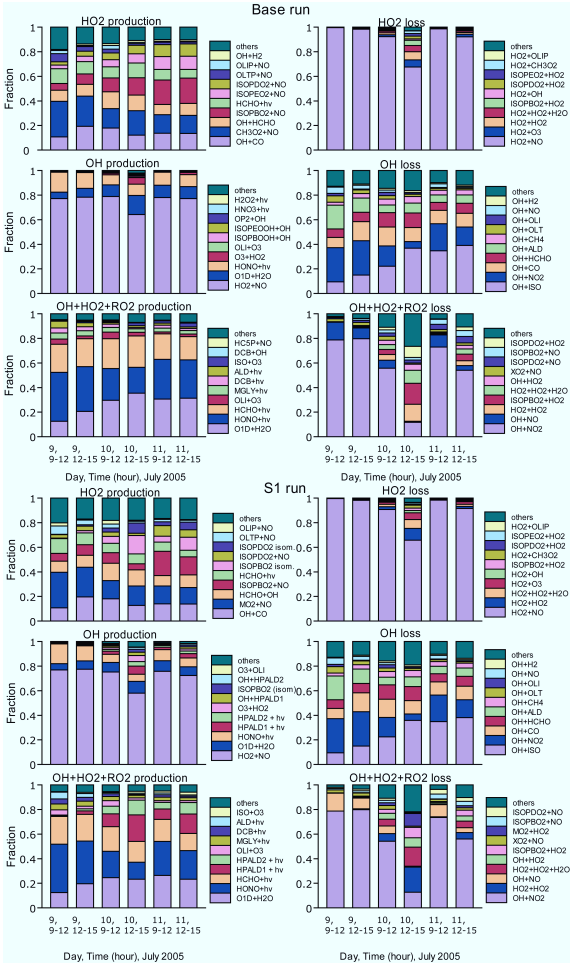

Fig. 4. Breakdown of production and loss processes of OH, HO_2, and radical group ($OH + HO_2 + RO_2$) in the base and S1 runs.

ACPD
11, 28851–28894, 2011

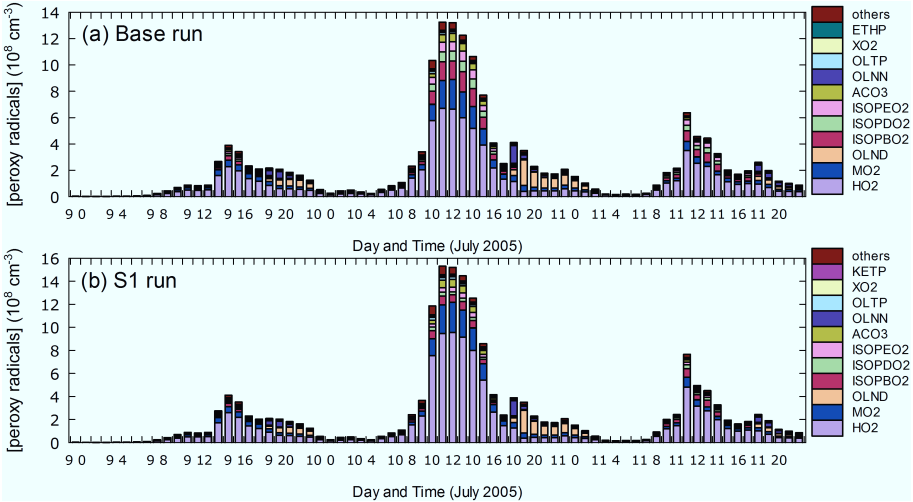

Fig. 5. Breakdown of peroxy radicals (HO_2 and RO_2) in the base and S1 runs. MO2, OLND, OLNN, ACO3, OLTP, ETHP, KETP, and XO2, stand for methyl peroxy radical, NO_3–alkene adduct (reacting via decomposition), NO_3-alkene adduct (reacting to form HO_2), saturated acylperoxy radicals, peroxy radicals from OLT (terminal olefins), peroxy radicals from ethane, peroxy radicals from ketones, and parameterized peroxy radicals accounting for additional NO to NO_2 conversions, respectively.

ACPD
11, 28851–28894, 2011

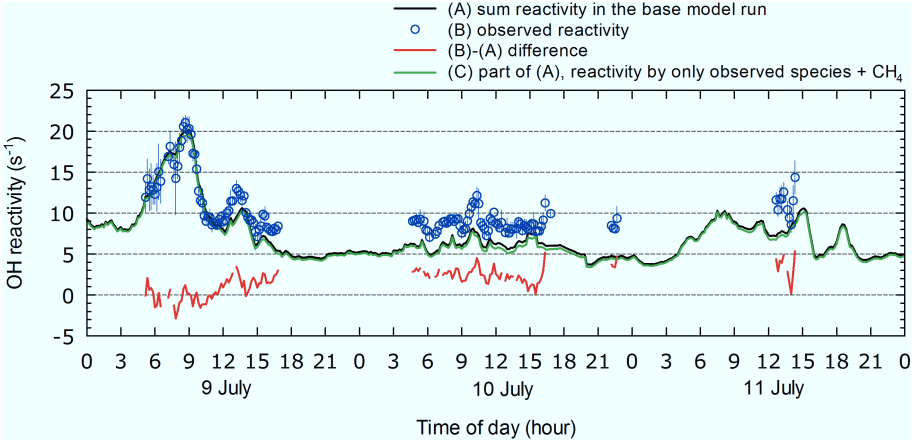

Fig. 6. OH reactivities observed by Tokyo Metropolitan University group (B, blue) compared with the sum of OH reaction rates with respect to all chemical species (A), including those measured and others calculated in the base run (black). Green (C) shows the fraction of calculated reactivities attributable to reactions with observed species (including methane). The difference between the observed (B) and modeled total (A) reactivities is shown in red; this is used as a basis for calculating amounts of additional hydrocarbon assumed in further model runs.

ACPD
11, 28851–28894, 2011

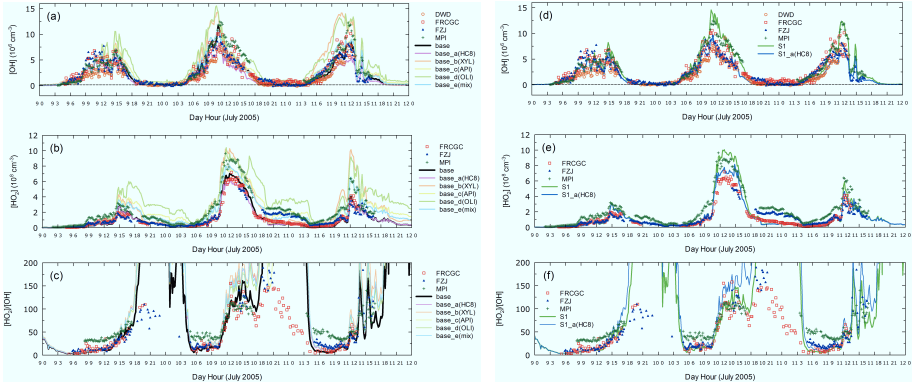

Fig. 7. Comparisons of observed and modeled **(a)** OH and **(b)** HO_2 concentrations, and **(c)** HO_2/OH ratios. The results from the base run and its variants (Base_a(HC8), Base_b(XYL), Base_c(API), Base_ d(OLI), and Base_e(mix)) are shown; **(d–f)** are the same as **(a–c)**, but showing the results from the S1 and S1_a(HC8) runs.

ACPD
11, 28851–28894, 2011

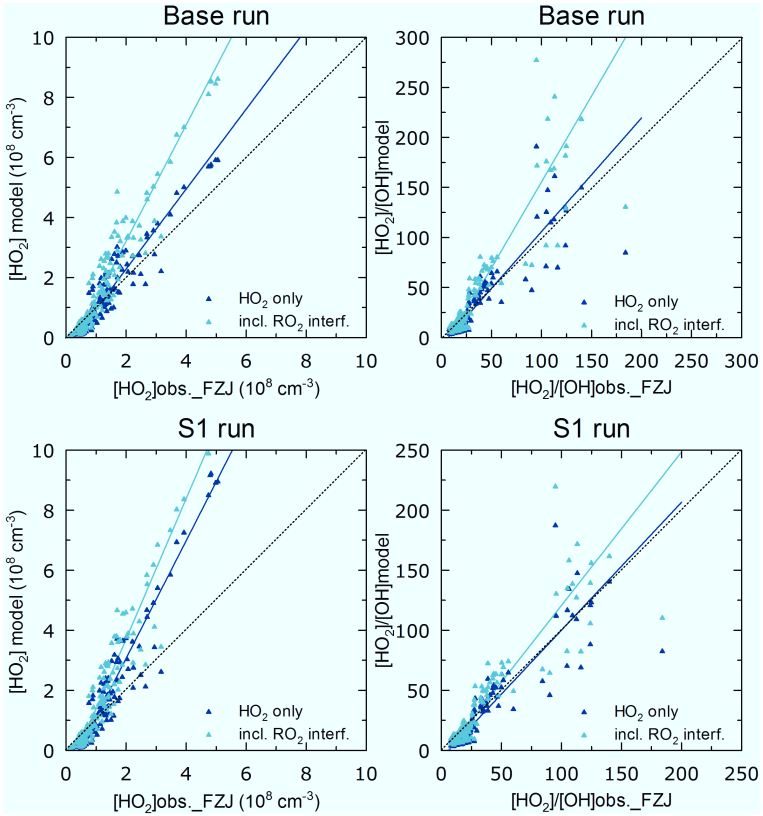

Fig. 8. Scatterplots between HO_2 and HO_2/OH ratios observed by FZJ instrument and those modeled, without taking RO_2 interference into account (HO_2 only, dark blue), and taking the interference into account (i.e., on the basis of HO_2(*), light blue). The results are shown for the base run (upper panels) and S1 run (lower panels).

ACPD
11, 28851–28894, 2011

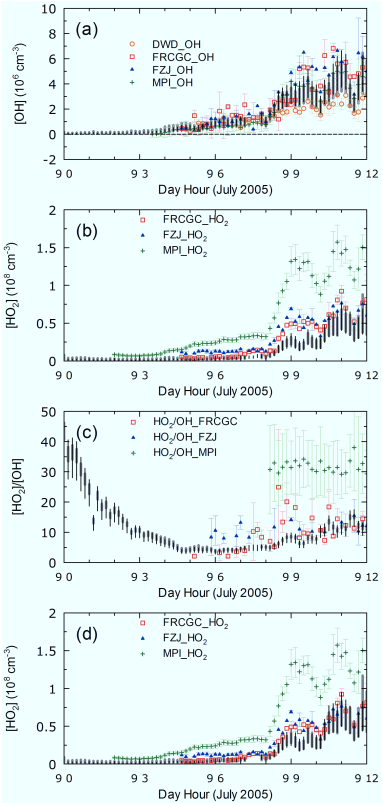

Fig. 9. Comparisons of observed and modeled **(a)** OH and **(b)** HO_2 concentrations, **(c)** HO_2/OH ratios, and **(d)** HO_2(*) concentrations with the full range of model ensemble results (gray bars) and uncertainty range (1σ) of the base run (black bars) on the morning of 9 July. The colored error bars represent 1σ ranges of observations during 10 min and do not represent systematic uncertainties of the observations.

ACPD
11, 28851–28894, 2011

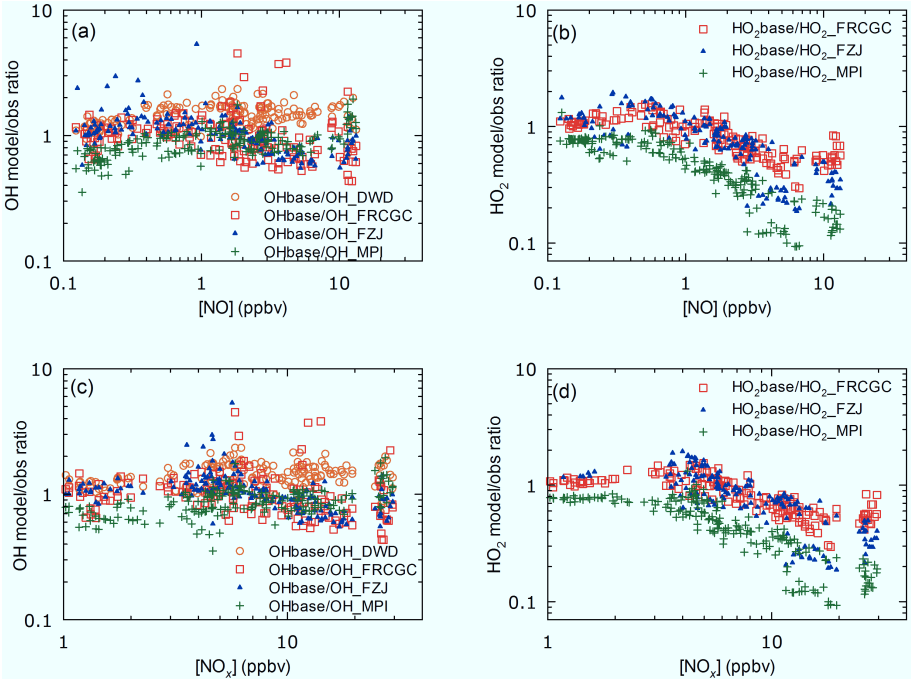

Fig. 10. Model/observation ratios for OH (left) and HO_2 (right) as functions of NO and NO_x concentrations for the base run. Only daytime (06:00–18:00 UTC) data are used.

ACPD
11, 28851–28894, 2011

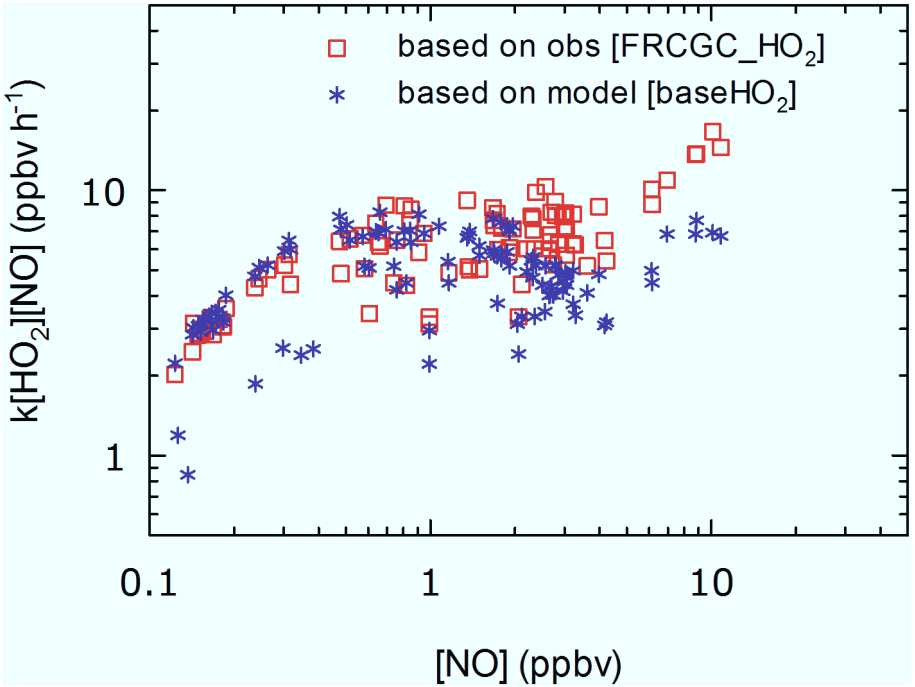

Fig. 11. $HO_2 + NO$ reaction rates derived from HO_2 observed by FRCGC instrument (red squares), and HO_2 modeled by the base run (purple stars) plotted as a function of NO. Only midday (09:00–15:00 UTC) data are used.

ACPD
11, 28851–28894, 2011